Modelling railway ballasted track settlement in vehicle-track interaction analysis

Ilaria Grossoni (1), William Powrie (2)*, Antonis Zervos (2), Yann Bezin (1), Louis Le Pen (2)

(1) Institute of Railway Research, University of Huddersfield, Huddersfield, UK

(2) University of Southampton, Southampton, UK

* corresponding author

Abstract

The geometry of a ballasted railway gradually deteriorates with trafficking, mainly as a result of the plastic settlement of the track-bed (ballast and sub-base). The rate and amount of settlement depend on a number of factors, and for various reasons are difficult to predict or estimate analytically. As a result, various empirical equations for estimating the rate of development of plastic settlement of railway track with train passage have been proposed. A review of these equations shows that they (i) do not reproduce the form of settlement *vs* number of load cycles relationships usually seen in the field; (ii) do not reflect current knowledge of the behaviour of soil subgrades in cyclic loading; and (iii) are often critically dependent on the curve fitting parameters used, which in turn depend on the circumstances in which the calibration data were obtained. To address these shortcomings, this paper develops a semi-analytical approach, based on the known behaviour of granular materials under cyclic loading, for the calculation of plastic settlements of the trackbed with train passage. The semi-analytical model is then combined with a suitable vehicle-track interaction analysis to calculate rates of development of permanent settlement for different initial trackbed stiffnesses, vehicle types and speeds. The model is shown to be able to reproduce recursive effects, in which a deterioration in track geometry causes an increased variation in dynamic load, which feeds back into a further deterioration in track geometry. The new model represents a significant improvement on current empirical equations, in that it is able to reproduce observed aspects of railway track settlement on the basis of the known behaviour of soils and ballast in cyclic loading.

Keywords

1. Introduction

For nearly 200 years, most of the world's railways have run on ballasted track. With trafficking, the geometry of a ballasted track gradually deteriorates, mainly as a result of the plastic settlement of the track-bed (ballast and sub-base). Intuitively, and as demonstrated by experimentation, the rate and amount of settlement would be expected to depend on a number of factors, including [1]:

- The loads imposed, including type and amount of traffic (e.g. axle load, speed, vehicle dynamic effects, cumulative tonnage);

- The track superstructure characteristics (e.g. rail and sleeper type, sleeper spacing, rail-pads and any additional resilient layers such as under-sleeper pads), which influence the distribution of loads into the underlying ballast and ground;
- The ballast, sub-ballast and sub-grade layer characteristics (e.g. depth, density, stiffness or resilient modulus, ballast specification in terms of particle size distribution and mineralogy, ballast contamination, drainage and pore water pressure conditions), and the ability of these supporting layers to resist cyclic loading.

When geometry defects become too severe, maintenance – usually in the form of automated tamping or manual packing – is carried out to realign the track and enable the continued safe running of trains. Unfortunately, tamping may also disrupt the load-bearing structure [2] and damage individual ballast grains, resulting in a diminishing return period between maintenance interventions until eventually the track-bed requires full renewal [3].

Four major difficulties in predicting the development of settlement are that:
1. On well-performing track, the rate of accumulation of residual (plastic or permanent) settlement with each loading cycle is almost vanishingly small (in the order of a nanometre); classical soil mechanics theories are not well-suited to modelling such small settlements and their gradual accumulation over potentially millions of loading cycles.
2. Settlement may be attributable to either the ballast or the subgrade, and most likely to both [4]. Different types of subsoil and ballast will have different tendencies to settle; even for ballast having the same grading (particle size distribution curve) and mineralogy, the settlement may depend on factors such as the depth of ballast, shoulder slope and the sleeper type and sleeper / ballast interface conditions (e.g. the use or absence of under sleeper pads) [5, 6].
3. Settlement generally arises as a result of both densification (volume change) and lateral spreading (shear deformation) of the ballast and subgrade [5, 6].
4. It is generally differential (rather than uniform) settlements that cause the track geometry to deteriorate to the extent that it needs maintenance [7]. The development of differential settlement can only be replicated in an analysis if there are pre-defined initial differences, for example in trackbed stiffness and / or in loading, that are not usually initially obvious in reality. There is ample evidence from foundation engineering of a correlation between the maximum settlement and the angular distortion – that is, larger settlements generally are likely to be associated with larger differential settlements [8, 9].

These difficulties have led to the development of empirical ballast settlement equations as discussed later, although such equations often do not take account explicitly of differences in sub-base, ballast type and geometry, sleeper type or even loading conditions (axle load and speed).

Recent developments in modelling railway track system behaviour have focused on implementing differentially deteriorating track support conditions in vehicle-track dynamic interaction analyses (e.g. [10-13]), with the short-term dynamics of vehicle-track interaction (e.g. [14, 15]) linked to the long-term degradation of the track through an iterative procedure. The approach is usually based on a time domain simulation of vehicle-track interaction in which the force transmitted by the track system (superstructure) to the supporting layers is calculated at each sleeper position and then used

as input into a settlement equation for track geometry degradation prediction [1]. However, there is no consensus on which ballast settlement equation to use. This is unsurprising, because the equations are empirical and their applicability depends on prevailing conditions including traffic type, track structure type and ballast condition.

The aims of this paper are to
- review current ballast settlement equations, the range of variables and parameters they can take into account, and the conditions for which they were derived
- develop an alternative semi-analytical approach to estimating track support system settlement, based on established soil mechanics principles and referenced to field and full scale laboratory test data
- demonstrate the implementation of the proposed approach in a vehicle-track dynamic interaction analysis model to calculate rates of differential track settlement and track geometry deterioration, and compare it with previous methods.

2. Current ballast settlement equations

A prerequisite to an improved ability to predict the development of differential settlement along a section of track is a better understanding of the relationship between plastic settlement and loading, based on the relevant properties of the ballast and the subgrade at a local scale. Ideally, a ballast settlement equation would be able to account for the effects of the
1. number and magnitude of load cycles
2. train speed (allowing for dynamic load)
3. subgrade separately from the ballast
4. condition of the ballast, subgrade and the interface with the track.

Many, if not all, of these factors are acknowledged within track geometry prediction tools used by industry to plan maintenance over route-scale lengths of track. For example, the T-SPA module within VTISM [16] modifies the basic ballast settlement equation through two main factors. These are the "Local Track Section Factor" (LTSF), which scales the empirical track geometry deterioration equation to the locally measured rate; and the "Ballast Condition Factor" (BCF), which attempts to replicate the observed reduction in the time interval between successive maintenance tamps, generally held to be the result of fines from tamping-damaged ballast grains filling the voids. There are also equations in the literature that attempt to link the development of track geometry deterioration (standard deviation from the desired level) to these factors directly (e.g. [17]). However, these are few and are outside the scope of this paper, which focuses on estimating the rate of track settlement at the level of individual sleepers.

Most authors, including Sato [17] and Dahlberg [18], speculate that there are two major stages of ballasted track settlement, occurring as a result of cumulative loading expressed in million gross tonnes (MGT) or, more usually, the number of cycles of an (often assumed constant) load:
1. Stage 1: after tamping, settlement occurs initially relatively rapidly with MGT or number of cycles as the ballast grains rearrange to establish a structure capable of carrying the applied external loads. This is characterised by a reduction in void ratio and a densification of the ballast [17], i.e. volumetric effects dominate

2. Stage 2: settlement occurs at a slower rate, increasing approximately linearly with MGT or number of cycles. This is attributed to a variety of causes, including the lateral movement of the ballast, penetration of the ballast into the subgrade, and ballast grain breakage and abrasion [18]. Essentially, non-volumetric effects (including shear / lateral spreading) dominate.

2.1. Basic equations

Most of the equations that have been proposed to characterise track settlement are empirical. Many take one of two forms:

1. Logarithmic or "ORE-type": $S_N = S_0.(1 + C.log_{10}N)$ or $S = S_0.(1 + C.lnN)$ (e.g. ORE 1970 [19], Shenton [20], Stewart [21]); or

2. Exponential or "Selig type": $S_N = S_0.N^a$ (e.g. Selig [4], Indraratna [22], Cuellar [23]) where S_N is the settlement after N load cycles, S_0 is the settlement after one loading cycle, and C and a are empirically-determined constants. Slightly more complex expressions are given by, for example, Jeffs [24], Thom [25] and Indraratna [26].

The more commonly used or cited track settlement equations are summarised in Appendix 1; some of these were reviewed in [18]. A review of empirical permanent deformation models for soils in the context of pavement and railway design was recently presented in [27].

Many equations relate the settlement after N load cycles to the settlement after the first cycle, either explicitly or by inference. Arguably, this is a way of taking into account at least implicitly a range of factors including the load per cycle, assuming that this remains constant. Other equations take into account of a number of factors explicitly, such as the stiffness, condition or nature of the ballast and in some cases the subgrade.

Three problems with these types of equations are that

1. they do not reproduce the form of settlement *vs* number of load cycles relationships usually seen in large scale laboratory tests or in the field

2. the outcomes are critically dependent on the curve fitting parameters used, which in turn depend on the circumstances in which the calibration data were obtained

3. those expressed in terms of the number of loading cycles do not generally account for the effect of differing axle loads. (Equations expressed in terms of MGT may do, but assume – probably unrealistically – that the effect of an increase in load is linear).

The second of these points is illustrated in Figure 1, which compares the settlement calculated after 100,000 cycles using the example ballast settlement equations indicated in Table 1 with the curve fitting parameters proposed by the original authors, categorised according to the type of test on which they are based.
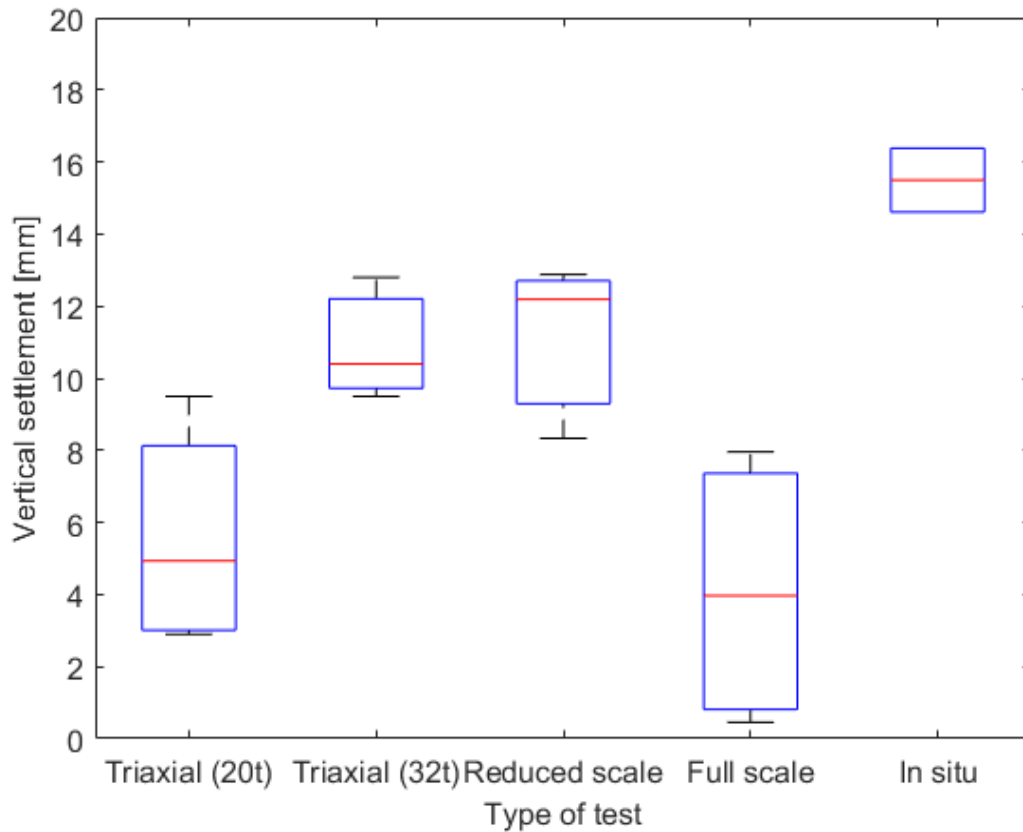
Figure 1: Comparison of settlement results obtained at 100,000 cycles using the equations in Table 1. For each box, the central mark indicates the median, and the bottom and top edges of the box indicate the 25th and 75th percentiles, respectively

Table 1: Summary of settlement equations used in the preparation of Figure 2, categorised according to the source of the data on which they are based (triaxial test, reduced or full scale ballast box, field measurements)

Author	Equation type	Equation	Equivalent axle load [t]	Maximum / minimum axle load per cycle [t]	Basis of equation
Shenton [20]	Logarithmic	$\varepsilon_N = 0.016 \cdot (1 + 0.2 \cdot \log_{10} N)$	20	20 / 0	Triaxial tests on ballast specimens with 20 tonne equivalent axle load
Guérin [28]	-	Settlement curve	20		
ORE [19]	Logarithmic	$\varepsilon_N = 0.00156 \cdot (100n - 38.2) \cdot (1 + 0.2 \cdot \log_{10} N)$	20		
Alva-Hurtado [29]	Logarithmic	$\varepsilon_N = 0.0116 \cdot (0.85 + 0.38\log N) + 0.000134 \cdot (0.05 - 0.09\log N)$	20		
Shenton [20]	Logarithmic	$\varepsilon_N = 0.0156 \cdot (1 + 0.2 \cdot \log_{10} N)$	32	32 / 0	Triaxial tests on ballast

5

ORE [19]	Logarithmic	$\varepsilon_N = 0.00345 \cdot (100n - 38.2) \cdot (1 + 0.2 \cdot \log_{10} N)$	32		specimens with 32 tonne equivalent axle load
Alva-Hurtado [29]	Logarithmic	$\varepsilon_N = 0.0156 \cdot (0.85 + 0.38\log N) + 0.000243 \cdot (0.05 - 0.09\log N)$	32		
Steward [21, 30]	Logarithmic	$\varepsilon_N = 0.0156 \cdot (1 + 0.29 \cdot \log_{10} N)$	20		Reduced scale ballast box test
Indraratna [22, 31]	Logarithmic	$S_N = 2.31 \cdot (1 + 0.345 \cdot \log_{10} N)$	25	23.3 / 5	
Indraratna [26]	Logarithmic	$S_N = 0.5 \cdot (1 + 0.43\log N + 0.8\log N^2)$	25		
Thom [25]	Logarithmic	$S_N = (\log_{10} N - 2.4)^2$	20		Full scale ballast box test
Cedex [23]	Exponential	$S_N = 0.07 N^{0.1625}$	17	19 / 3	
Abadi [32]	-	Settlement curve	20		
Partington [33]	Logarithmic	$S_N = 0.29 \log_{10} N^{1.77}$	22	24 / 4	In situ measure-ments
Fröhling [34]	-	Settlement curve	26		

Figure 1 shows large discrepancies between the calculated settlements, both within and between each category of experimental basis. In most cases, the discrepancies between categories are intuitively unsurprising. The in situ settlements are largest, but potentially include a contribution from the subgrade, which none of the laboratory measurements do. The equations based on triaxial tests simulating a 20 tonne axle load and the full-scale ballast tests are reasonably consistent; both include only the ballast settlement and the equivalent axle loads are the same. The equations based on parameters from triaxial tests simulating a 32 tonne axle load give greater settlements than those based on triaxial tests simulating a 20 tonne axle load, which again seems intuitively reasonable. The only counter-intuitive difference between categories of equation is that the calculations based on reduced scale ballast box tests seem rather high.

Within an individual category, the variation is greatest for the equations based on triaxial tests simulating a 20 tonne axle load and full scale ballast box tests. It is not clear why this should be, but the potential variability of test specimens, the number of datasets involved and factors such as the frequency of loading could all potentially have an influence. Figure 1 highlights the important influence of the conditions under which a settlement equation and its associated parameters have been derived. Harmonisation would require the development of either a common test procedure that takes into account the effects of vehicle-track interaction, or a modelling approach built up by considering the fundamental behaviour of each of the system components.

2.2. More complex equations

In tests carried out to millions of cycles, data of track settlement *vs* number of load cycles generally

show two inflexion points [6, 35, 36] as indicated in Figure 2, which also shows approximately the phases identified by Sato and Dahlberg. A simple logarithmic or exponential relationship is unable to reproduce this form of curve. (Interestingly, data from a large scale test rig simulating 4 million cycles of high speed train loading presented by Zhang et al, 2019 [37], do not show the second inflexion point and do conform reasonably well to a simple Shenton-type logarithmic equation).

To improve the fit with experimental data exhibiting both phases of behaviour characterised by two inflexion points on the logarithmic graph, more complex equations are needed. Figure 2 shows curve fits from two empirically determined equations able to match a second downturn in the settlement rate on a log scale. The first of these (referred to as the Okabe equation or fit) was originally proposed in [38] (in the same form as that more recently presented in [17]); it combines logarithmic and linear terms (Equation 1):

$$S_N = (C_1 - C_2 \cdot e^{-\alpha N}) + \beta N \qquad \text{(Equation 1)}$$

where S_N is the settlement at cycle N, N is the number of loading cycles (or cumulative MGT), and C_1, C_2, α and β are empirically-determined coefficients.

A more complex equation was proposed in [39], based on vibration experiments on columns of confined glass particles, and was fitted by [40] to ballast settlements measured in ballast / sleeper tests carried out to a relatively low number of cycles (10,000), in which the ballast was confined horizontally (Equation 2).

$$S_N = S_1 + S_2 \left[1 - \frac{1}{1 + \alpha ln \left(1 + \frac{N}{N_0} \right)} \right] \qquad \text{(Equation 2)}$$

where S_1 is the settlement measured after the first cycle and S_2, α, N_0 are curve-fitting parameters with arguable physical meanings.

Equation 2 was developed for settlement occurring solely as a result of densification and is not able to reproduce the later downward phase shown in tests to millions of cycles, which is probably attributable mainly to lateral ballast spreading at the sleeper ends / ballast shoulder. To allow for lateral spreading at higher cycles, Equation 2 can be modified by adding the βN term from Equation 1 to create Equation 3: this is the second equation plotted in Figure 2, referred to as the modified fit.

$$S_N = S_1 + S_2 \left[1 - \frac{1}{1 + \alpha ln \left(1 + \frac{N}{N_0} \right)} \right] + \beta N \qquad \text{(Equation 3)}$$

Using algorithms to determine the constants, Equation 3 can be fitted to data from laboratory sleeper settlement tests to 3 million cycles (Figure 2). However, the large number of constants of Equation 3 means that there is no unique best fit solution, so it is necessary to constrain the permissible ranges of some of the constants. Different stages of settlement are apparent in both the data and the fitted curves shown in Figure 2, with Equation 3 achieving very good fits. However, whether the components / constants of Equations 1 and 3 individually represent different stages of ballast settlement, and indeed the underlying mechanisms responsible, remains a matter of conjecture. A further feature of these equations (and most if not all of the others reported in

Appendix 1) is that they are not inherently dimensionally consistent; hence the curve fitting constants have to have units (dimensions) that make them so.
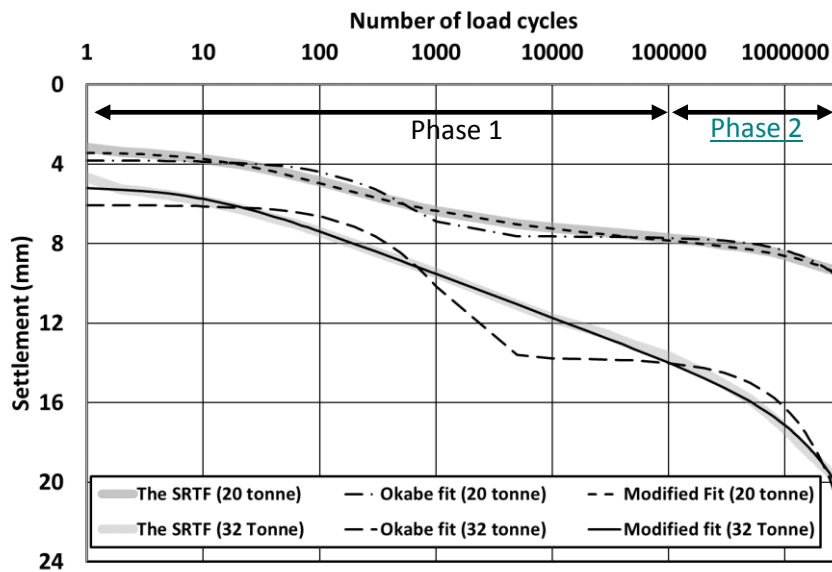

Figure 2: Form of the relationships between track settlement and number of load cycles given by the Okabe equation (Equation (1), [38]) and a modified version proposed in [39, 40].

2.3. Equations suitable for use in VTI modelling

Vehicle-track interaction (VTI) modelling offers an efficient way of calculating dynamic wheel-rail contact forces and the displacement, velocity and acceleration of each part of the vehicle and the track system as trains travel along the track. Usually, the vehicle is described as a multi-body system with lumped masses, linked through linear or non-linear force connectors (usually, springs and dashpot dampers). The track is modelled using finite element (FE) theory for the rail as a beam and concentrated masses for the sleepers, with the subgrade support represented by springs and dashpots. Different support system properties may be specified for each sleeper to represent longitudinal variation of support stiffness [41]. Short to medium (1 m to 70 m) wavelength rail roughness, relevant for VTI analysis at train speeds up to about 200 km/hr, is modelled on the basis of actual track recording car measurements along a particular stretch of railway. Different initial horizontal levels may therefore be specified at each sleeper position. In the calculation of long term settlements using VTI analysis, each sleeper position can be adjusted as the track irregularity grows, to capture the effects on vehicle dynamics and wheel-rail interaction forces. It is usually computationally too expensive to change the levels of the sleepers following every train passage; developing differential settlement may be replicated adequately by changing the sleeper levels, for example every 1000 train passes.

Settlement equations suitable for use in VTI modelling should be able to reproduce the main observed features of behaviour, without having so many curve-fitting parameters as to result in a non-unique fit. A further requirement is that the input parameter(s) for the settlement equation, such as load applied and track system response (displacements, accelerations, forces, etc.), can be calculated by the VTI model at each loading cycle, capturing both the traffic characteristics and the longitudinal variability of the track. Not all of the equations in the literature fit these criteria; many incorporate these factors within fixed parameter that have been calibrated for a particular case

study. The equations proposed by Guérin [28], Sato [42] and Fröhling [34] have been selected for further study as they do meet the criteria. They are described briefly below.

2.3.1. Guérin's equation

Guérin [28] carried out an extensive series of tests at a loading frequency of 30 Hz, representing approximately the tenth harmonic of the car passing frequency at a train speed of 215 km/h. (For a discussion of the relationship between frequencies of loading, train speed and train geometry, see [43] or [44]). The results suggested that the rate of accumulation of permanent settlement of the ballast may be expressed as a function of the current maximum sleeper deflection:

$$\frac{dS_N}{dN} = 1.44 \cdot 10^{-6} \cdot d_{b,max}{}^{2.51}$$
(Equation 4)

where N is the number of cycles and $d_{b,max}$ the maximum elastic sleeper deflection. $d_{b,max}$ is a function of N, and expression of Equation 3 in non-differential form would require the ability to specify and integrate this function.

The numerical values of the parameters in Equation 3 proposed by Guérin were for the particular circumstances of the tests used to obtain the baseline data. More recently an extension in the applicability of the formula to train speeds in excess of 350 km/h and "normal" or "soft" soil has been proposed [45]. A major drawback of the Guérin formulation is that it is ill-adapted to a change in track configuration, because the ratio of plastic deformation to maximum displacement will likely change with varying ballast type, depth, etc. There is also a dimensional inconsistency owing to the exponent applied to $d_{b,max}$.

.

2.3.2. Sato's equation

Sato [42] presented a two part equation (Equation 5 & 6) for settlement as a function of the number of load cycles N and the ballast pressure P or ballast force F. The settlement S_N depends on whether a threshold stress P_{th} has been exceeded:

$$S_N = \begin{cases} a \cdot F^b \cdot c \cdot N \\ d \cdot (P - P_{th})^2 \cdot e \cdot N \qquad if\ P > P_{th} \end{cases}$$
(Equation 5)
(Equation 6)

where the coefficients a and c depend on the power b. The coefficients d and e and the pressure threshold P_{th} depend on the ballast layer thickness (Table 2 and Figure 3).
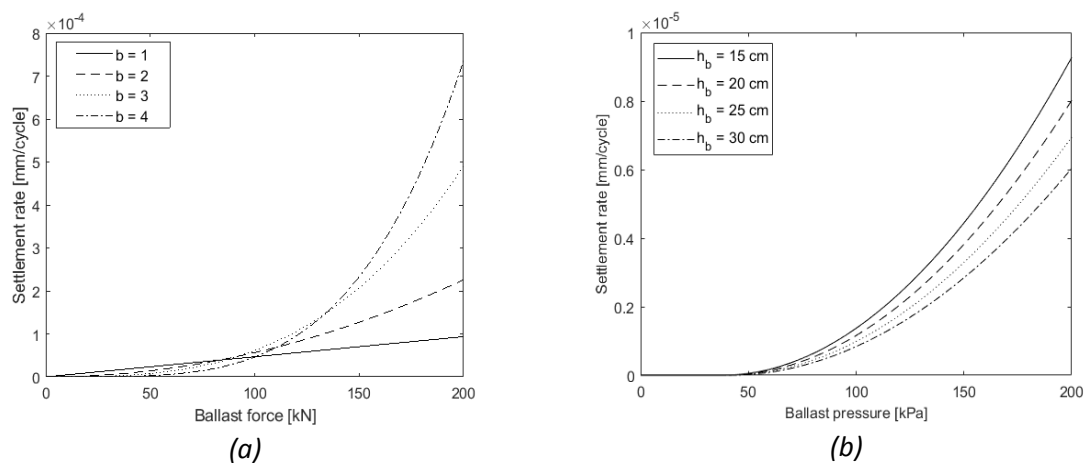

(a)   *(b)*

Figure 3: Settlement rate according to (a) Eq. 5 and (b) Eq. 6 [42] *vs* sleeper-ballast interface force or pressure

Table 2: Parameters used in Sato's equations [42]

Value of parameter b	Value of parameter a	Value of parameter c[1]
1	1.403×10^{-6}	0.33
2	9.411×10^{-9}	0.66
3	4.382×10^{-11}	1.40
4	1.839×10^{-13}	2.50

Value of parameter d	Ballast depth h_b, cm	Threshold stress P_{th}, kPa	Value of parameter e
2.70×10^{-10}	15	37.5	1.30
	20	38.6	1.14
	25	39.6	1.00
	30	40.6	0.88

Sato's use of different equations above and below the threshold strain reflect the importance of stress dependent non-linear soil behaviour. However, the equations contain dimensional inconsistences and the settlements calculated are sensitive to the stress threshold used. The threshold stress must be assumed to increase with stiffness, otherwise a stiffer trackbed support leads to higher stress transfer from the track superstructure onto the ballast and consequently higher calculated settlements, which is contrary to general experience [46]. The main input parameter for Equation 4, the stress on the ballast, may be computed at each step in a vehicle-track interaction analysis.

2.3.3. Fröhling's equation

By analysing measured data of average track settlement with accumulating traffic, Fröhling [34] developed an expression that, while logarithmic in form [10], also takes account of the deviatoric stress at the sleeper-ballast interface by adjusting the local stiffness, and dynamic load amplification at the wheel-rail interface (Equation 7):

$$S_N = \left\{ \left[K_1 + K_2 \cdot \left(\frac{k_{2mi}}{K_3} \right) \right] \cdot \frac{P_{dyn}}{P_{ref}} \right\}^{w} \cdot \ln N \qquad \text{(Equation 7)}$$

where S_N is the total settlement after N loading cycles; k_{2mi} is the measured average track stiffness (MN/m) at a particular sleeper; K_1, K_2, K_3, are constants with units of kPa, m^{-1} and no units respectively; P_{dyn} (kN) is the dynamic wheel load; P_{ref} (kN) is the reference wheel load used in the simulation; and w is an exponent. For the case analysed by Fröhling using GEOTRACK with a reference wheel load of 13 t, K_3 = 1.34, K_1 = 194 kPa, K_2 = -1.96 mm^{-1} and w = 0.3. These parameters were determined over a range of track stiffnesses 60 MN/m $\leq k_{2mi} \leq$ 132 MN/m. At track stiffnesses > 132 MN/m the expression in square brackets becomes negative, resulting in an increase in calculated settlement with track stiffness (Figure 4) that does not match observed behaviour.

---

[1] This apparently spurious parameter is included to reflect the original reference.
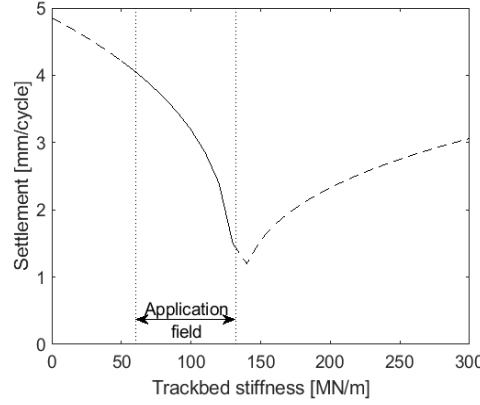
Figure 4: Variation of settlement predictions with trackbed stiffness using the Fröhling equation within (-)_and without (--) the defined limits.

The input variables P_{dyn} and k_{2mi} can be determined as outputs from each step of a VTI analysis, but Equation 7 does have dimensional inconsistencies.

3. Proposed semi-analytical approach

The review of equations currently used to estimate railway track settlement are mainly empirical; do not incorporate a subgrade behaviour consistent with modern soil mechanics understanding and principles (a point also evident in [27]); do not generally account for differences in axle load; and do not reproduce patterns of settlement with trafficking seen in the field. In this section, a new model for calculating ballast settlements is proposed, which is based on the observed behaviour of soils in cyclic loading, is sensitive to axle load as well as cumulative loading, and is able to reproduce the observed behaviour of ballast under cyclic loading.

In the following, σ is the vertical stress and the total strain $\varepsilon = \varepsilon^e + \varepsilon^p$ comprises an elastic (reversible) component ε^e and a plastic (irreversible) one ε^p. Using a superposed dot to denote increments of a quantity and assuming linear elasticity, elastic strain increments are calculated as $\dot{\varepsilon}^e = \frac{\dot{\sigma}}{E^e}$, where E^e is the elastic modulus. We define the plastic strain increment $\dot{\varepsilon}^p$ directly, using a rate equation that fulfils the following requirements:

- $\dot{\varepsilon}^p$ is an increasing function of $\dot{\sigma}$, so that larger stress increments cause larger plastic strain increments
- Failure occurs at a limiting or ultimate value of stress σ_u; we assume $\dot{\varepsilon}^p \to \infty$ as $\sigma \to \sigma_u$.
- Plastic strain develops only during loading, and only if the stress exceeds a threshold $\sigma_t \leq \sigma_u$
- $\dot{\varepsilon}^p$ is an increasing function of the difference $(\sigma_u - \sigma_t)$, so that the greater the margin by which the threshold stress is a exceeded, the larger the corresponding plastic strain increment.

An expression satisfying these requirements is:

$$\dot{\varepsilon}^p = \frac{1}{A} \cdot \left(\frac{\sigma - \sigma_t}{\sigma_u - \sigma} \right) \cdot \dot{\sigma} \qquad \text{(Equation 8)}$$

where A is a material parameter with units of stress, which is interpreted as a plastic modulus. This expression was arrived at heuristically, and is potentially the simplest one satisfying the above requirements while introducing only one additional parameter.

Consecutive load cycles of equal magnitude are known to result in progressively smaller increments of plastic strain, hence σ_t must also increase with loading. It is therefore assumed that σ_t is a function of an internal parameter k, loosely quantifying how the properties of the material change during the course of deformation; it is assumed that $k \equiv \varepsilon^p$ as a first approximation. However, $\sigma_t \leq \sigma_u$ always; hence σ_t must increase at decreasing rate with ε^p. In addition, other things being equal, a higher elastic modulus E^e would be expected to be associated with a higher σ_t and a higher σ_u.

A general expression that satisfies the above requirements is:

$$\sigma_t = \sigma_{t,ref}(\varepsilon^p) \cdot \left[1 - C \left(1 - \frac{E^e}{E^e_{ref}} \right) \right] \qquad \textbf{(Equation 9)}$$

where $\sigma_{t,ref}(\varepsilon^p)$ captures the dependence of σ_t on the plastic strain, while the square bracketed term takes into account the (assumed linear) dependence of σ_t on the elastic stiffness. E^e_{ref} is a reference value of the elastic stiffness and C a constant calibration parameter. Further, the data support the assumption that $\sigma_{t,ref}$ is a simple hyperbolic function $\sigma_{t,ref}(\varepsilon^p) = (\alpha_1 \cdot \varepsilon^p + \alpha_2)/(\alpha_3 \cdot \varepsilon^p + 1)$ where α_1, α_2 and α_3 are calibration parameters. The hyperbolic function can be defined fully by three constraints. Assuming that, for $E^e = E^e_{ref}$, $\sigma_{t,0}$ and h^p_0 are the initial values of the threshold stress and its first derivative respectively, and $\sigma_{u,ref}$ the value of the ultimate stress, yields:

$$\sigma_{t,ref}(\varepsilon^p) = \frac{h^p_0 \cdot \sigma_{u,ref} \cdot \varepsilon^p + \sigma_{t,0} \cdot \left(\sigma_{u,ref} - \sigma_{t,0} \right)}{h^p_0 \cdot \varepsilon^p + \sigma_{u,ref} - \sigma_{t,0}} \qquad \textbf{(Equation 10)}$$

(Equation 9 and (Equation 10 imply that the ultimate stress varies with elastic stiffness as:

$$\sigma_u = \sigma_{u,ref} \cdot \left[1 - C \left(1 - \frac{E^e}{E^e_{ref}} \right) \right] \qquad \textbf{(Equation 11)}$$

This is reasonable, in that a higher peak strength and stiffness are both characteristics of dense or overconsolidated soils. In other words, the stiffness and the strength of a soil would be expected to be correlated, with a stiffer soil also being stronger. For any given soil, the value of the C parameter could be determined on the basis of triaxial tests at different void ratios or preconsolidation stresses, as appropriate for the type of soil and the relevant field conditions.

Informed by Equation 9 for σ_t, the two equations for $\dot{\varepsilon}^e$ and $\dot{\varepsilon}^p$ can be integrated numerically using the trapezium rule to determine the elastic, plastic and total strain response corresponding to any given stress history. Integrating over a typical load cycle $\sigma_1 \rightarrow \sigma_2 \rightarrow \sigma_1$ using 20 increments was found to provide good resolution and accuracy for the stress-strain response.

Although integrating each load cycle is not onerous, in the sense that results for tens of thousands of cycles on a single sleeper can be produced within a few minutes on a desktop computer, implementing this as part of a vehicle-track interaction analysis over a length of track with hundreds of sleepers leads to a significant computational burden. It is desirable to carry out the integration more efficiently, if possible within a single computational step for each load cycle, even at the expense of a loss of accuracy. Assuming that a load cycle $\sigma_1 \rightarrow \sigma_2 \rightarrow \sigma_1$ increases the plastic strain from ε^p_1 to ε^p_2, for known ε^p_1, ε^p_2 can be calculated as:

$$\varepsilon_2^p = \varepsilon_1^p + \int_{\sigma_1}^{\sigma_2} \frac{1}{A} \cdot \frac{1}{\sigma_u - \sigma} \cdot \left(\sigma - \sigma_t(\varepsilon^p, E^e)\right) \cdot d\sigma \qquad \text{(Equation 12)}$$

Taking the Taylor expansion of $\sigma_t(\varepsilon^p, E^e)$, keeping the first (constant) term so that $\sigma_t(\varepsilon^p, E^e) \cong \sigma_t(\varepsilon_1^p, E^e)$, and carrying out the algebra, eventually leads to:

$$\varepsilon_2^p \cong \varepsilon_1^p + \frac{1}{A} \cdot \left[(\sigma_u - \sigma_1) \cdot ln\left(\frac{\sigma_u - \sigma_1}{\sigma_u - \sigma_2}\right) - (\sigma_2 - \sigma_1)\right] \qquad \text{(Equation 13)}$$

Using this approximation results in a loss of accuracy in the order of 5%, which is more than compensated for by the observed two orders of magnitude increase in the speed of calculation. Figure 5 shows, as an example, the form of the cyclic stress-strain behaviour calculated using Equations 8-11, for stresses ranging between σ_1 = 0 kPa and σ_3 = 65 kPa with parameter values A = 10^6 kPa, C = 1.0, E^e = 10^9 kPa , $E_{ref}^e = 10^9$ kPa, and $\sigma_{u,ref}$ = 69.2 KPa. The evolution of the threshold stress with increasing number of cycles is also shown. It may be seen that Equations 8-11, to which Equation 13 provides an approximate solution, capture the typical behaviour of a soil-type material in cyclic uniaxial loading. The detail of the behaviour might vary at high frequencies and displacements if inertial effects (accelerations) become significant, or evolve with load cycling as a result of material degradation e.g. grain breakage. These issues have not been explored in this paper (and indeed are generally neglected in the literature), but could in principle be taken into account to some extent through suitable testing and parameter value selection.
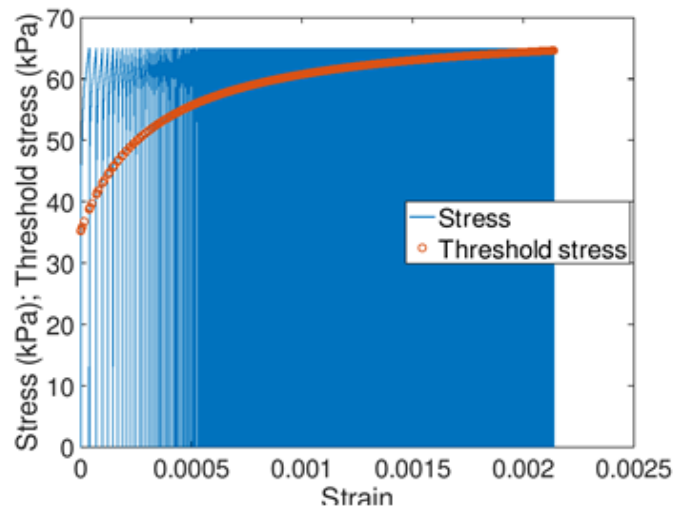

Figure 5: Typical calculated stress-strain response and corresponding evolution of threshold stress in a calculation using the semi-analytical model.

In the following sections, the proposed model is implemented in vehicle-track interaction analyses and compared with the empirical equations identified in section 2.3.

4. Implementation of settlement equations in vehicle-track interaction analyses

4.1. Overview

The methodology adopted to link the short-term (during train passage) and long-term (permanent settlement) ballast behaviour through vehicle-track interaction analysis was described, using the Sato and Guérin equations, in [12], and is summarised in Figure 6. Here, it is expanded to encompass the proposed semi-analytical approach and the Fröhling equation. Results using all four approaches are then compared using data from a case study with varying support stiffness [12].
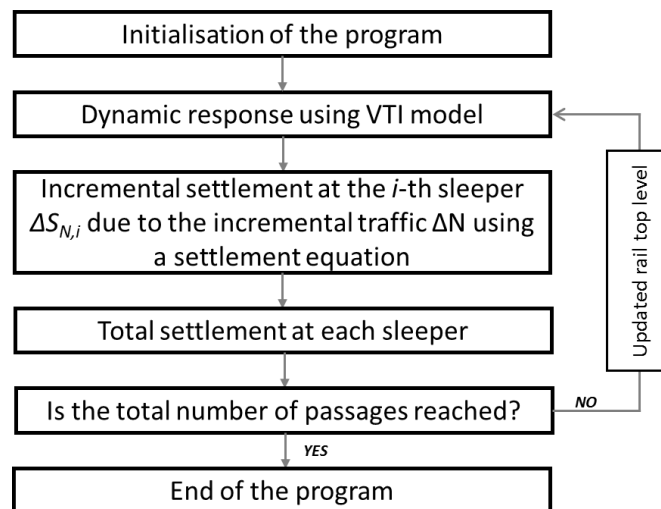
```
┌─────────────────────────────────────────────┐
│         Initialisation of the program        │
└─────────────────────────────────────────────┘
                      ↓
┌─────────────────────────────────────────────┐
│       Dynamic response using VTI model       │◄──────┐
└─────────────────────────────────────────────┘       │
                      ↓                                 │
┌─────────────────────────────────────────────┐       │
│  Incremental settlement at the i-th sleeper  │    ┌──┴──────────────┐
│ ΔS_{N,i} due to the incremental traffic ΔN using │ │ Updated rail top │
│           a settlement equation              │    │      level        │
└─────────────────────────────────────────────┘    └──┬──────────────┘
                      ↓                                 │
┌─────────────────────────────────────────────┐       │
│        Total settlement at each sleeper      │       │
└─────────────────────────────────────────────┘       │
                      ↓                                 │
┌─────────────────────────────────────────────┐  NO   │
│    Is the total number of passages reached?  ├───────┘
└─────────────────────────────────────────────┘
                      ↓ YES
┌─────────────────────────────────────────────┐
│             End of the program               │
└─────────────────────────────────────────────┘
```

Figure 6: General methodology used to iteratively link together the short-term and long-term ballast behaviour [12].

The vehicle-track interaction model is based on a finite element (FE) description of a rail as a beam on discrete supports at each sleeper location using support characteristics (linear stiffness and damping terms) that can vary along the length of the track. A quarter vehicle, with half a bogie and two wheels, is considered. Wheel-rail contact is described using non-linear Hertzian theory [41]. The numerical model is integrated in the time domain to calculate train movement and track reaction force.

The dynamic contact loads (hence pressures for the semi-analytical equation) between each sleeper and the ballast (for Sato's equation), the wheel-rail contact force (for Fröhling's equation) and the maximum sleeper displacements (for Guérin's equation) were determined in the time domain for the entire duration of the vehicle passage, and then used as input to the relevant settlement calculation. The track level is quantified at each sleeper position from the incremental settlement ΔS for the traffic loading step ΔN. The vertical rail geometry is updated to include the incremental settlement at each sleeper location and the next dynamic simulation is executed, until the maximum number of cycles is reached. The wheel-rail force and sleeper-ballast interface forces then follow from the multi-body dynamics VTI calculation for the given track geometry configuration (rail irregularity plus sleeper settlement). The parameter ΔN, which defines how many simulations are carried out for a given total number of cycles N, is chosen on a case-by-case basis as a trade-off

between accuracy and computational costs. The total settlement is evaluated as the sum of the settlement reached at the previous iteration and the incremental settlement in the current step of ΔN cycles.

Parameter values for the semi-analytical model were determined with reference to single sleeper settlement tests in the Southampton Railway Testing Facility (SRTF) [6]. For the other empirical models, the parameter values specified in the original references were adopted. For the avoidance of doubt, the equations or methods investigated and the parameter values applied in this comparison work are summarised in Table 3.

Table 3: Input parameters for the equations in VTI analyses

Guérin (Eq. 3)	Sato (Eq. 4)		Fröhling (Eq. 6)		Semi-analytical model	
$\dfrac{dS_N}{dN} = 1.44 \cdot 10^{-6} \cdot d_{b,max}{}^{2.51}$	$S_N = a \cdot P^b \cdot N$		$S_N = \left\{ \left[K_1 + K_2 \cdot \left(\dfrac{k_{2mi}}{K_3} \right) \right] \cdot \dfrac{P_{dyn}}{P_{ref}} \right\}^w \cdot \ln N$			
Parameter values as in Eq. 3 above	a	4.365	K_1	194 kPa	Ultimate stress, σ_u	1120 kPa
	b	4	K_2	1.96 m $^{-1}$	Initial threshold stress, $\sigma_{t,0}$	140 kPa
			K_3	1.34	Initial plastic modulus	102380.4 kPa
			P_{ref}	See Table 4	C	0.5
			w	0.3	A	10^6 kPa

4.2. Simplifications

Distribution of the load by the sleepers into the trackbed depends on the applied load, the bending stiffness of the sleeper and the rails and the effective support stiffness, which may vary along the sleeper length. Stresses tend to concentrate directly under the rail seats [20], but the effective sleeper-ballast contact area depends on a number of factors including the ballast specification, sleeper material and the presence of additional layers such as under sleeper pads [47]. To avoid the difficulties associated with defining the exact nature of the sleeper-ballast interface, the stress on the ballast, the deflection and the load are considered herein as either averages over the sleeper footprint or as the gross value applied to the sleeper. Using the VTI model, it is possible to calculate the force at the rail-pad and the force at the ballast surface at each support position considered. The stress averaged over the total sleeper / ballast contact area (per half sleeper or sleeper end) is then calculated as:

$$\sigma = \frac{F_b}{A_s/2}$$

<div align="right">(Equation 14)</div>

where F_b is the force (from a single rail) at the ballast level and A_s is the area of the sleeper soffit.

5. Results from two case study sites

5.1. Case study 1

"Site B" in [12] has been used in this case study to show the influence of the trackbed stiffness on the long-term ballast behaviour. The original dataset was modified slightly to give stiffness values within the range 60 to 132 MN/m, consistent with Fröhling's assumptions (Figure 7). Two half vehicles typical of the site, i.e. a Class 91 electric locomotive and a laden freight vehicle, were modelled using the parameters given in Table 4.

Table 4: Vehicle and trackbed input parameters, Case study 1.

Parameter	Class 91 locomotive	Laden freight vehicle
Axle load	20 tonnes	22.5 tonnes
Unsprung mass	1300 kg	1350 kg
Speed	200 km/h	80 km/h
Total number of sleepers	80	80
Mean trackbed stiffness[2]	109.7 MN/m/sleeper end	
Trackbed stiffness SD[3]	14.9 MN/m/sleeper end	
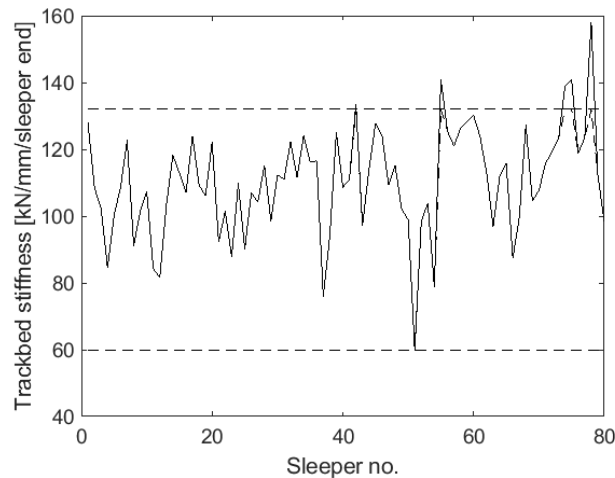
Figure 7: Trackbed stiffness distribution, case study 1: original distribution and modified distribution to limit the trackbed stiffness to between 60 and 132 MN/m

In total, eight simulations (2 vehicle types × 4 settlement models) were carried out.

---

[2] For the original dataset, the mean trackbed stiffness was 110.4 kN/mm (0.6% difference)

[3] For the original dataset, the trackbed stiffness standard deviation was 16.2 kN/mm (8.7% difference)
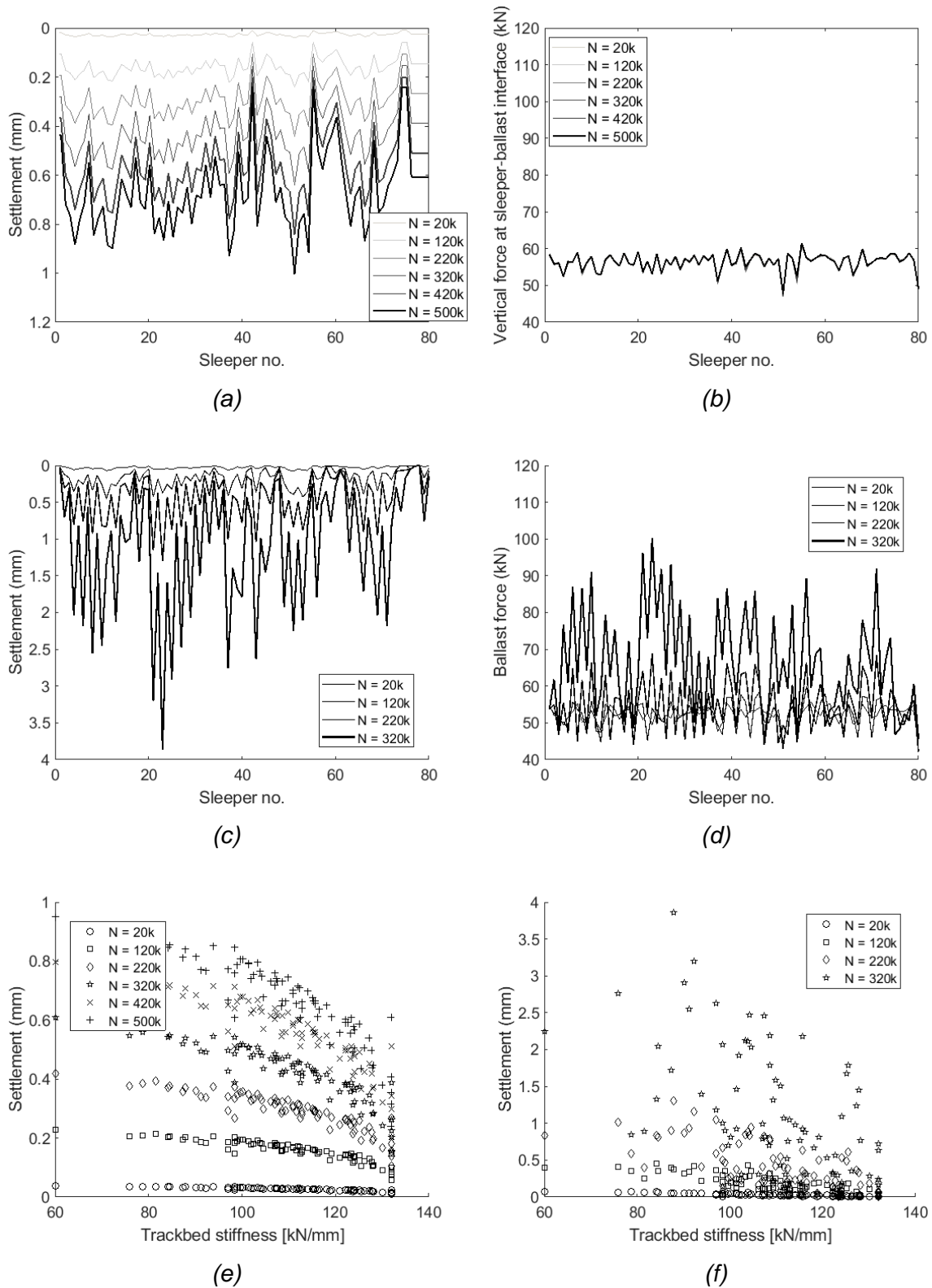
(a)

(b)

(c)

(d)

(e)

(f)

Figure 8 shows, for the Class 91 vehicle, an example of the evolution with increasing number of load cycles of the calculated track settlement below each sleeper (Figure 8 a & c) and the resulting distribution of ballast forces (Figure 8 b & d), according to the Fröhling (Figure 8 a & b) and the semi-analytical (Figure 8 c & d) settlement models. In this case the semi-analytical approach gives much faster settlement rates, with peak values after 320,000 cycles being three (mean) to six (maximum)

17

times those of Fröhling. In the modelling reported in this paper, the increased settlement is fed back directly as an increased track roughness at rail level; this is the approach most commonly adopted in the literature – see for example [34, 48, 49]. However, it leads to much greater dynamic load amplification and variation in load from sleeper to sleeper as indicated by the increased noisiness in forces seen in Figure 8 d for the semi-analytical model. In contrast, Figure 8 b (using the Fröhling equation) remains practically unchanged through increasing settlement cycles. The increased variation in dynamic forces feeds back into further increased differential settlement and localised defects, indicated by the series of deep troughs that initiate and growth with trafficking. Although the calculated track irregularity remains well within current maintenance intervention limits, even for Category 1 track in the UK, it probably highlights a shortcoming of the approach currently adopted in most coupled VTI settlement models of translating the settlement values as rail level irregularities, rather than introducing them as non-linearities between the sleeper and the ballast surface as in [7].
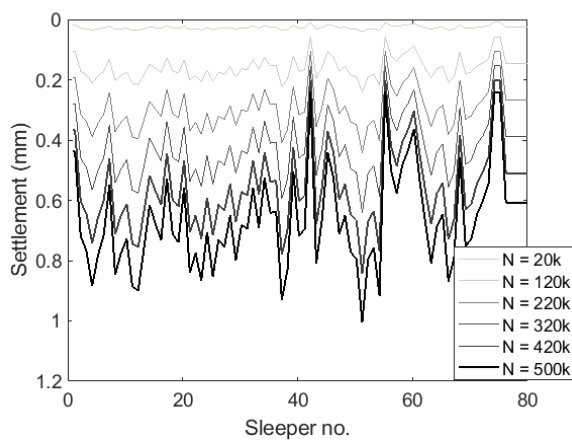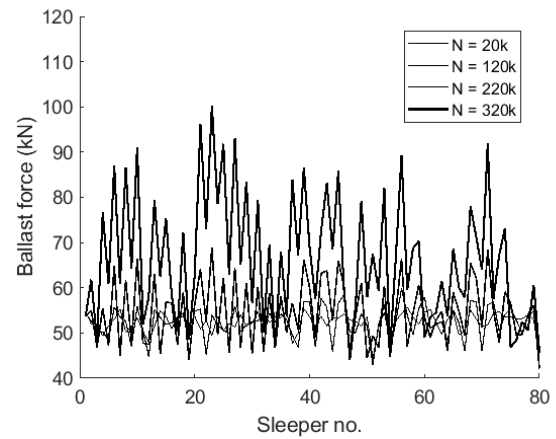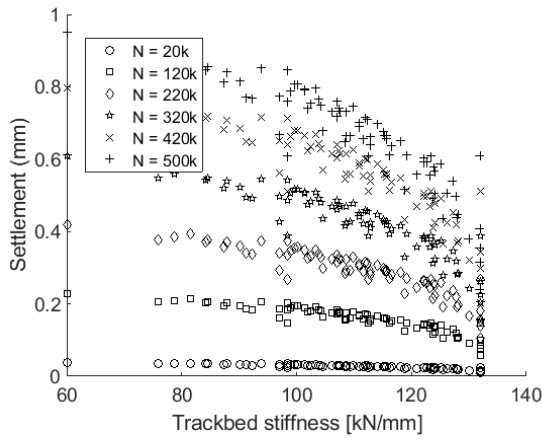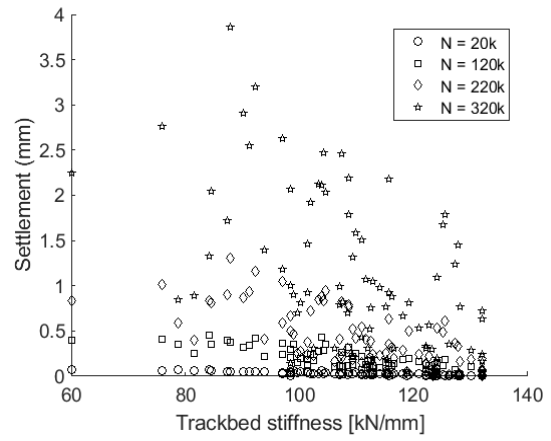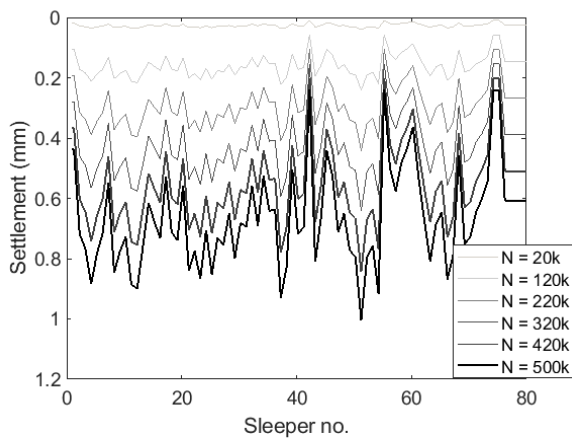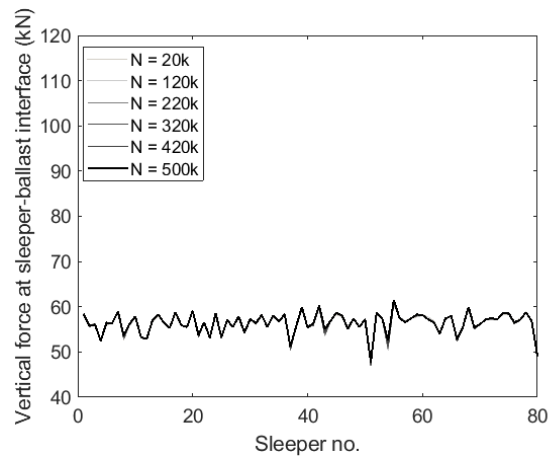

(a)
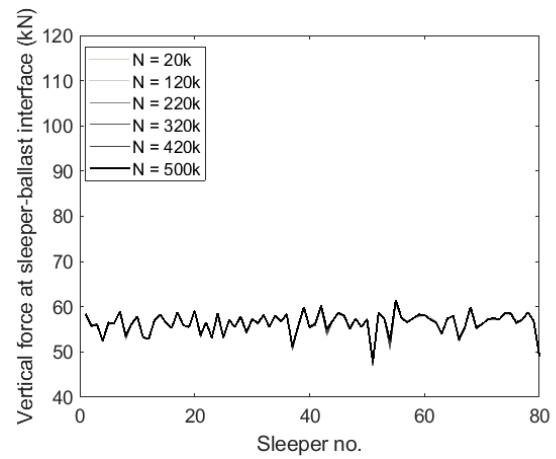
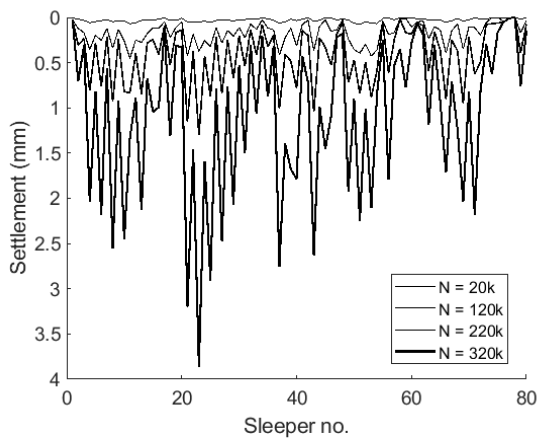*(b)*
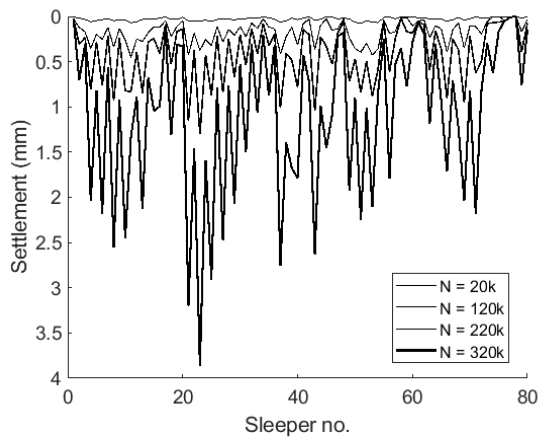
(c)

(d)

(e)

(f)

Figure 8: (a, c) Evolution in time of settlement below sleepers, (b, d) distribution of ballast forces for Class 91 vehicle and (e, f) settlement predictions against trackbed stiffness according to Fröhling's equation and the semi-analytical settlement model, respectively
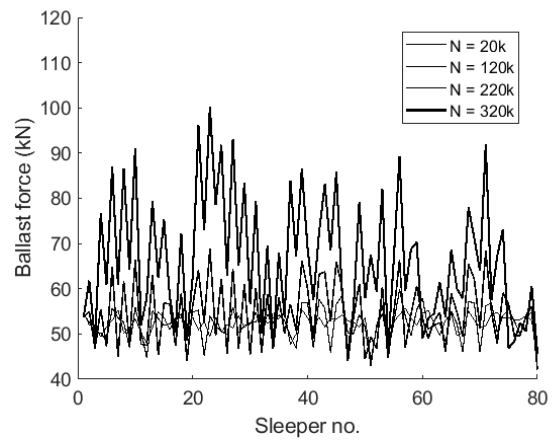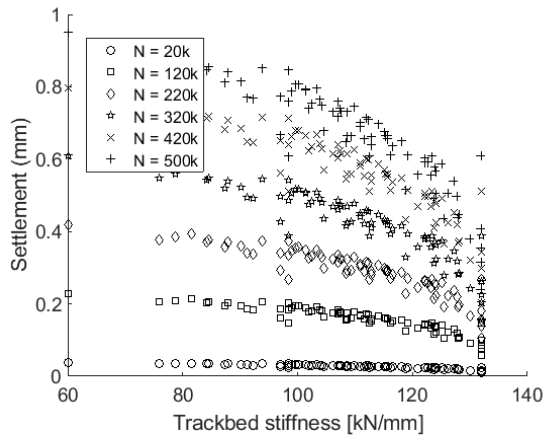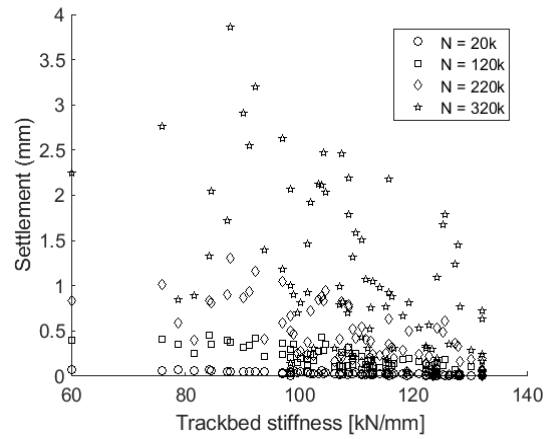

(a)

(b)

(c)

(d)

(e)   *(f)*

Figure 8 (e & f) shows that both approaches calculate lower settlement rates at locations with higher trackbed stiffness and vice versa. This is in line with expectations, as the rate of settlement calculated using Fröhling's equation is inversely proportional to the trackbed stiffness, while in the semi-analytical model the threshold stress is proportional to the trackbed stiffness. Settlements calculated using the semi-analytical approach show increasing scatter between individual sleepers with increasing number of cycles, owing to the amplification effect of such track irregularities on the dynamic loads as discussed above.
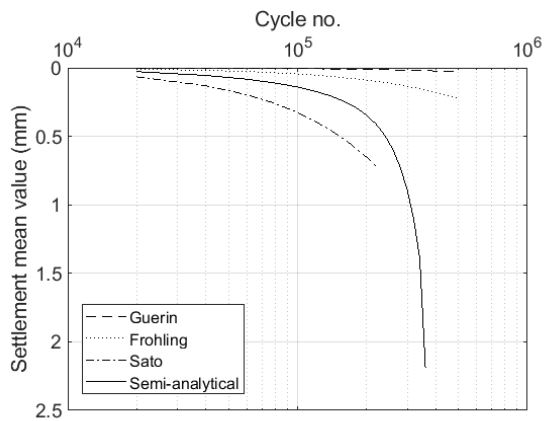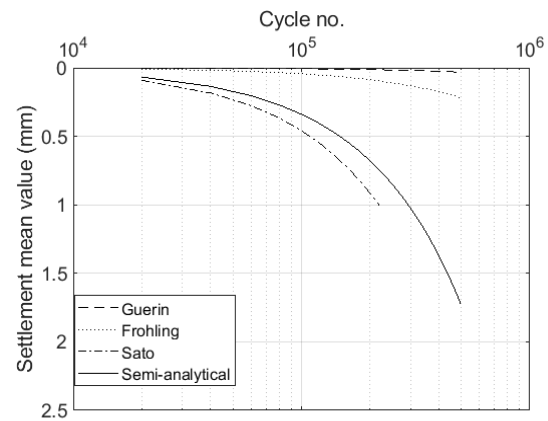
(a)   *(b)*

Figure 9 compares the development of the mean settlement with number of load cycles calculated by all four of the models, for both vehicle types considered.
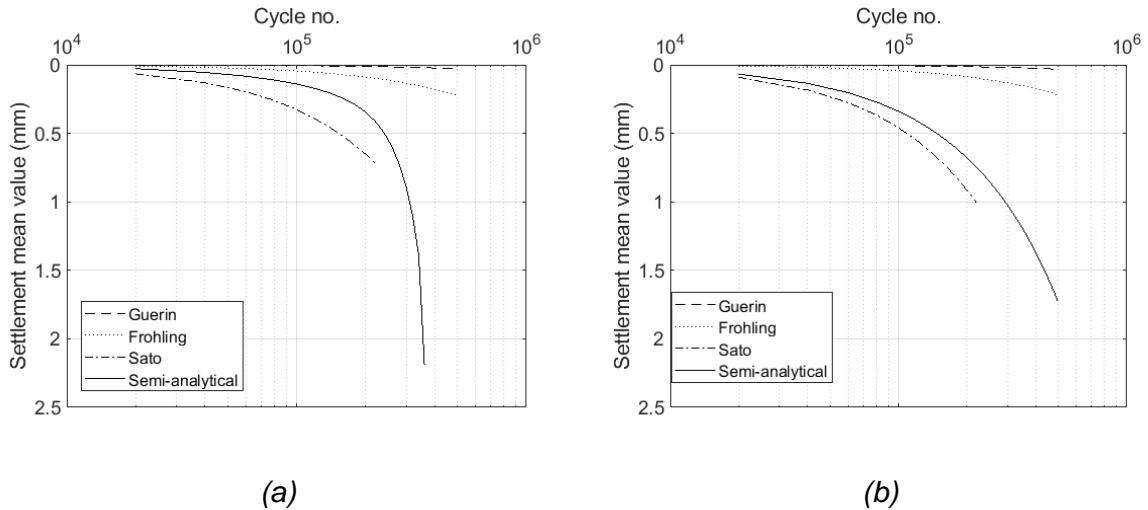
Figure 9: Comparison of mean settlements calculated with number of load cycles for (a) Class 91 and (b) freight vehicle

There is no significant difference between the settlements calculated using the Guérin and the Fröhling equations for the two vehicle types, i.e. these methods do not seem to be sensitive to the type and speed of vehicle and its dynamic interaction with the track. Furthermore, the settlements calculated using both of these approaches are very small – less than about 0.2 mm using Fröhling and less than 10% of this using Guérin, after 500 000 cycles. Sato's equation and the semi-analytical approach do show a difference between the responses to the two vehicle types. The higher speed and slightly lower axle load associated with the Class 91 locomotive appear to induce greater settlements than the heavier but slower freight wagon, probably owing to the load amplification discussed previously being greater at higher speed. In terms of magnitude, the calculated settlements of up to about 2 mm after 500 000 cycles are in the lowest quintile of the calculation methods based on full scale or field data shown in Figure 1, and about half those in the rig test data in Figure 2 for a 20 tonne axle load. These are at the low end of the generally reported range, but not unreaslistically low as is the case for the Guérin and the Fröhling equations.

In the case of the semi-analytical model, the load amplification calculated for the Class 91 locomotive is sufficient to cause the specified ultimate stress to be reached, and the relatively large increase in settlement with number of loading cycles is associated with failure of the trackbed. This will need to be refined in future studies to ensure that failure point is not reached unrealistically under expected track and vehicle running conditions.

5.1. Case study 2

Case Study 2 is based on the site presented in [50], with the vehicles indicated in Table 4 and the trackbed stiffness characteristics summarised in Table 5 and Figure 10. The trackbed stiffness distributions at the two case study sites are compared in Figure 11. The track stiffnesses at the second case study site are generally less than 60 MN/m/se, outside the range of applicability of Fröhling's equation, which is therefore not considered in this simulation.

Table 5: Main trackbed stiffness distribution characteristics in case study 2.

Parameter	Value

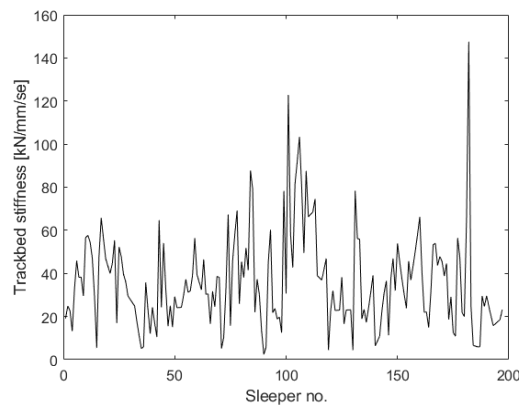|	
Total number of sleepers	*197*
Mean trackbed stiffness	*36.0 MN/M/sleeper end*
Trackbed stiffness SD	*22.1 MN/M/sleeper end*

Figure 10: Trackbed stiffness distribution in case study 2.
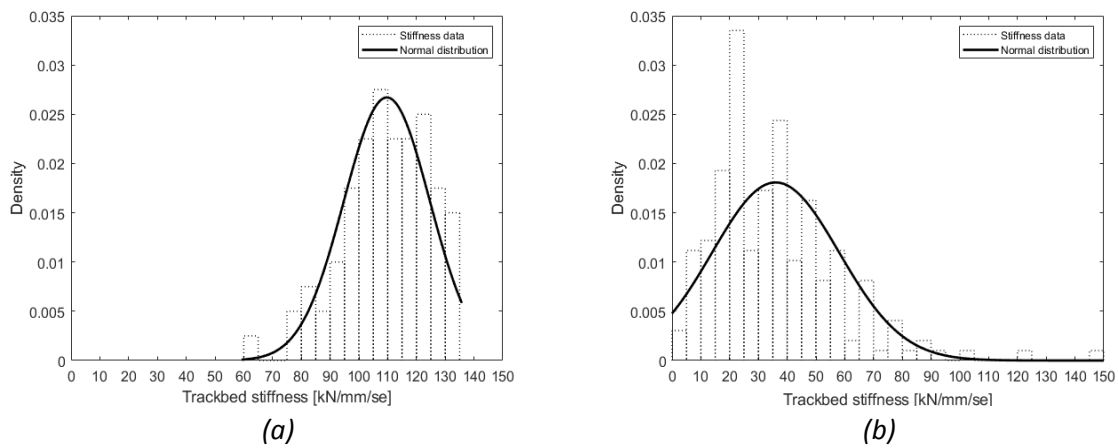

(a)   *(b)*

Figure 11: Comparison between trackbed stiffness distributions; (a) case study 1 and (b) case study 2.

The trackbed at Case study site 1 is on average about three times stiffer than at Case study site 2, with less variability. These differences are likely to be at least in part a consequence of the different trackbed stiffness measurement and calculation techniques used, as well as differing site conditions. At site 1, falling weight deflectomer measurements were made on unclipped sleepers, whereas at case study site 2 the effective trackbed stiffness was evaluated from analysis of sleeper movements during train passage and could have included the influence of how well individual sleepers were supported while connected to the rails. The FWD method is arguably an evaluation of the best case trackbed support whereas the latter method with trains present is a more accurate representation of how the track support system responds during train passage. While important, evaluating the most suitable measurement technique is outside the scope of this paper. Case study site 2, with a lower modelled trackbed stiffness, yields a higher mean settlement with greater variation (higher standard deviation) than Case study site 1.
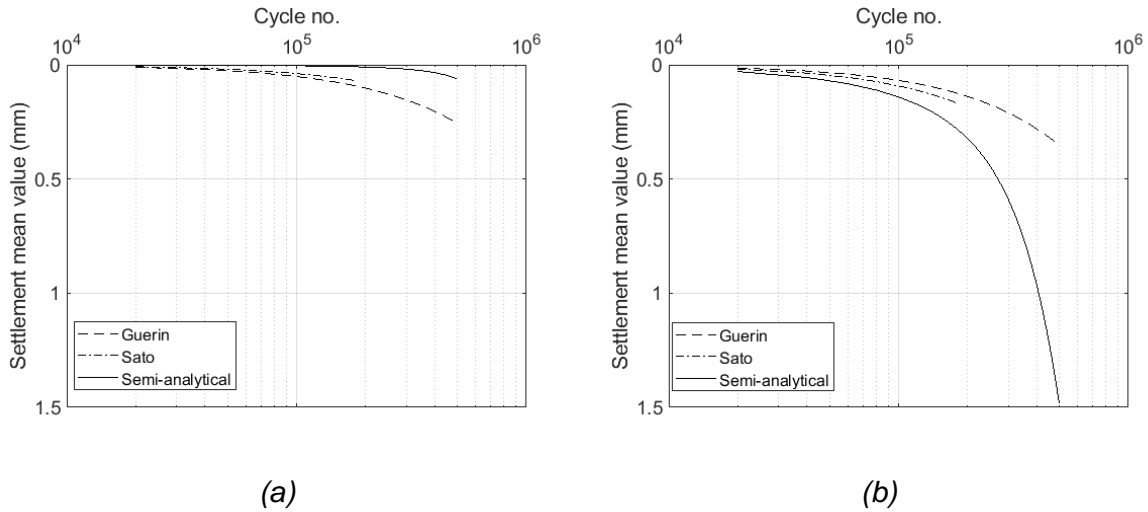
(a)   *(b)*

Figure 12 shows the curves of average settlement *vs* number of load cycles for both vehicle types, calculated for the stiffness distribution of Case Study 2 using the Guérin, Sato and semi-analytical approaches.

(a)   *(b)*
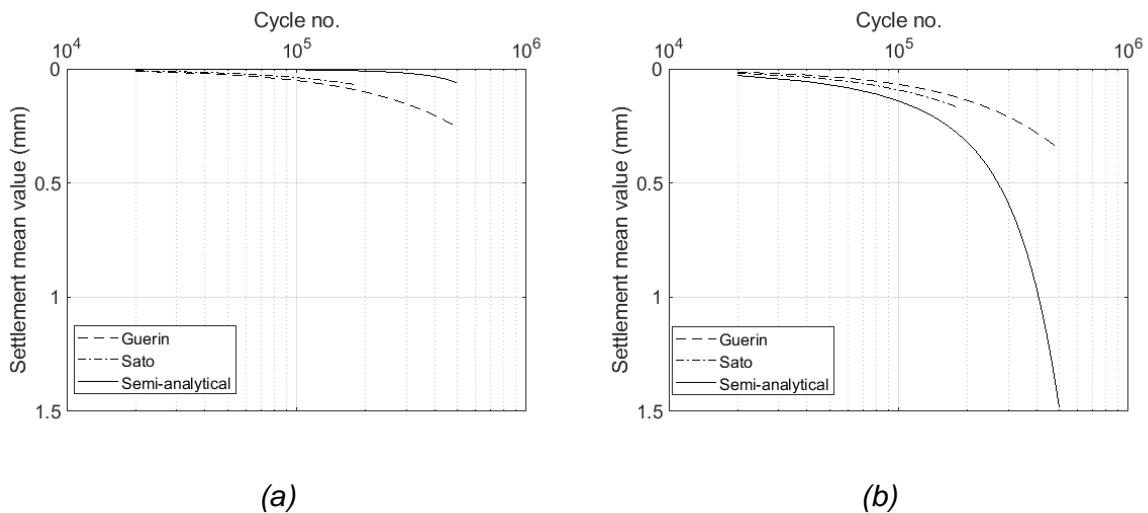
Figure 12: Comparison of mean settlement evolution calculated using the Guérin and Sato equations and the semi-analytical model for (a) Class 91 and (b) freight vehicle.

In this case, all three of the approaches considered show some differences between the calculated settlement curves for the two vehicle types, with the slightly heavier (but slower) freight vehicle giving rise to greater settlements than the Class 91 locomotive. The difference is particularly pronounced for the semi-analytical approach, which gives the smallest settlements for the Class 91 locomotive and the largest (up to the point of effective failure) for the freight wagon. It may be that the contrast between the modelled behaviour of the two sites, with speed being apparently more damaging than load at the first and vice versa at the second, is a result of the different trackbed stiffnesses (the first site being on average three times stiffer than the second). As in the first case study, the displacements are generally at or below the low end of the expected range. This illustrates that further work is needed to understand the physical significance, and obtain representative values of, the parameters used in the equations and models.

The semi-analytical model would benefit from being refined through the selection of parameters more suitable to each case study site. Nonetheless, it does have the potential to capture a range of different track behaviours that the more empirically-based equations do not. Realistic representation of the track in vehicle-track interaction analysis, and the calculation of track cumulative settlements as a result of train passage is in its infancy. The purpose of this paper has been to demonstrate the feasibility and potential of a soil mechanics based approach. Further work is needed, both to understand the physical meaning and quantify the parameters underlying the new model; and to validate the approach with reference to high quality, long-term datasets of track settlement, which at present are rare to non-existent.

6. Summary and conclusions

Equations that have been proposed to represent the gradual accumulation of plastic settlement of railway track with train passage have been reviewed. Three were selected for further study, on the basis that they are able to reproduce the main observed features of track settlement behaviour, and that they can take as inputs the outputs from an associated vehicle-track interaction model.

A semi-analytical expression, based on the known behaviour of granular materials under cyclic loading, has been developed. This expression is able to reproduce the accumulation of plastic settlement with each load cycle, with the amount of plastic settlement per cycle related to the stress in excess of a threshold stress. The threshold stress increases with the number of load cycles (work hardening), and with the initial stiffness of the trackbed. It also features an ultimate stress, at which plastic deformation continues unchecked.

When combined with a suitable vehicle-track interaction analysis, the semi-analytical model has been shown to be able to capture differences in the rate of development of permanent settlement as a result of differences in the initial trackbed stiffness, vehicle type and speed; and the development of rail roughness through differential settlement. It is also able to reproduce recursive effects, in which a deterioration in track geometry causes an increased variation in dynamic load, which feeds back into a further deterioration in track geometry.

While there remains considerable scope for refinement of the semi-analytical approach, particularly through the selection of parameter values appropriate to different site conditions, it shows considerable promise in being able to reproduce observed aspects of railway track settlement on the basis of the known behaviour of geomaterials (soils and ballast) in cyclic loading.

The work has also highlighted areas in which the vehicle-track interaction modelling approach needs improvement, in particular by applying the settlement growth at the interface between sleepers and the ballast, rather than as an equivalent rail irregularity as adopted in much of the current literature. Evaluation of the trackbed stiffness for input into such models also needs further research.

Acknowledgements

References

1.   In2Rail, *Deliverable D3.3: Evaluation of optimised track systems*. 2017.

2.   Aingaran, S., L. Le Pen, A. Zervos, and W. Powrie, *Modelling the effects of trafficking and tamping on scaled railway ballast in triaxial tests.* Transportation Geotechnics, 2018. **15**: p. 84-90.

3.   Lichtberger, B., *Track Compendium - Formation, Permanent way, Maintenance, Economics*. 2005, Hamburg: Eurailpress.

4.   Selig, E.T. and J.M. Waters, *Track geotechnology and substructure management*. 1994: Thomas Telford.

5.   Abadi, T., L. Le Pen, A. Zervos, and W. Powrie, *Effect of Sleeper Interventions on Railway Track Performance.* Journal of Geotechnical and Geoenvironmental Engineering, 2019. **145**(4).

6.   Abadi, T., L. Le Pen, A. Zervos, and W. Powrie, *Improving the performance of railway tracks through ballast interventions.* Proceedings of the Institution of Mechanical Engineers, Part F: Journal of Rail and Rapid Transit, 2016. **232**(2): p. 337-355.

7.   Nielsen, J.C.O. and X. Li, *Railway track geometry degradation due to differential settlement of ballast/subgrade – Numerical prediction by an iterative procedure.* Journal of Sound and Vibration, 2018. **412**: p. 441-456.

8.   Skempton, A.W. and D.H. MacDonald, *The allowable settlements of buildings.* Proceedings of the Institution of Civil Engineers, 1956. **5**(6): p. 727-768.

9.   Ricceri, G. and M. Soranzo, *An analysis on allowable settlement of structures.* Rivista Italiana di Geotecnica, 1985. **4**: p. 177-188.

10.   Frohling, R.D., *Deterioration of railway track due to dynamic vehicle loading and spacially varying track stiffness*, in *Faculty of Engineering*. 1997, University of Pretoria: Pretoria.

11.   Li, X., J.C.O. Nielsen, and B.A. Palsson, *Simulation of track settlement in railway turnouts.* Vehicle System Dynamics, 2014. **52**(Suppl.1): p. 421-439.

12.   Grossoni, I., A. Andrade, Y. Bezin, and S. Neves, *The role of track stiffness and its spatial variability on long-term track quality deterioration.* Proceedings of the Institution of Mechanical Engineers, Part F: Journal of Rail and Rapid Transit, 2019. **233**(1): p. 16-32.

13.   Nguyen, K., J. Goicolea, and F. Galbadón. *Dynamic effect of high speed railway traffic loads on the ballast track settlement*. in *Actas del Congresso de Métodos Numéricos em Engenharia (14/06/2011–17/06/2011), P*. 2011.

14.   Mosayebi, S.-A., J.-A. Zakeri, and M. Esmaeili, *Vehicle/track dynamic interaction considering developed railway substructure models.* Structural Engineering and Mechanics, 2017. **61**(6): p. 775-784.

15.   Zakeri, J.A. and M.R. Tajalli, *Comparison of Linear and Nonlinear Behavior of Track Elements in Contact-Impact Models.* Periodica Polytechnica Civil Engineering, 2018. **62**(4): p. 963-970.

16.   Serco, *VTISM analysis to inform the allocation of variable usage costs to individual vehicles* 2012.

17. Sato, Y., *Japanese studies on deterioration of ballasted track.* Vehicle System Dynamics, 1995. **24 Suppl.**(1): p. 197-208.

18. Dahlberg, T., *Some railroad settlement models—a critical review.* Proceedings of the Institution of Mechanical Engineers, Part F: Journal of Rail and Rapid Transit, 2001. **215**(4): p. 289-300.

19. ORE, *Question D 71 Stresses in the Rails, the Ballast and in the Formation Resulting from Traffic Loads.* 1970, Uthecht.

20. Shenton, M. *Deformation of railway ballast under repeated loading conditions*. in *Symposium on Railroad Track Mechanics, RRIS 01 130826, Publication 7602*. 1975.

21. Stewart, H. and E. Selig, *Correlation of Concrete Tie Track Performance in Revenue Service and at the Facility for Accelerated Service Testing - Volume II: Prediction and Evaluation of Track Settlement*. 1984, US Department of Transportation Federal Railroad Administration: Washington, DC.

22. Indraratna, B., M.A. Shahin, and W. Salim, *Stabilisation of granular media and formation soil using geosynthetics with special reference to railway engineering.* Journal of Ground Improvement, 2007. **11**(1): p. 27-44.

23. Cuellar, V., F. Navarro, M.A. Andreau, J.L. Camara, F. Gonzalez, M. Rodriguez, A. Nunes, P. Gonzale, R. Diaz, J. Navarro, and R. Rodriguez, *Short and long term behaviour of high speed lines as determined in 1:1 scale laboratory tests*, in *9th World Congress on Railway Research*. 2011: Lille.

24. Jeffs, T. and S. Marich, *Ballast characteristics in the laboratory*, in *Conference on Railway Engineering*. 1987, Institution of Engineers, Australia.

25. Thom, N. and J. Oakley, *Predicting differential settlement in a railway trackbed*, in *Railway foundations conference: Railfound*. 2006. p. 190-200.

26. Indraratna, B. and S. Nimbalkar, *Stress-strain degradation response of railway ballast stabilized with geosynthetics.* Journal of geotechnical and geoenvironmental engineering, 2013. **139**(5): p. 684-700.

27. Ramos, A., A. Gomes Correia, B. Indraratna, T. Ngo, R. Calçada, and P.A. Costa, *Mechanistic-empirical permanent deformation models: Laboratory testing, modelling and ranking.* Transportation Geotechnics, 2020. **23**: p. 100326.

28. Guerin, N., *Approche experimentale et numerique du comportement du ballast des voies ferrees*, in *Structures et materiaux*. 1996, Ecole nationale des ponts et chausses: Paris.

29. Alva-Hurtado, J.E. and E.T. Selig, *Permanent strain behavior of railroad ballast*, in *10th International Conference on Soil Mechanics and Foundation Engineering*. 1981: Stockholm (Sweden).

30. Stewart, H.E. and E. Selif, *Correlation of concrete tie track performance in revenue service and at the facility for accelerated service testing-Volume ii: Predictions and evaluations of track settlement*. 1984.

31. Indraratna, B., M.A. Shahin, and W. Salim, *Stabilisation of granular media and formation soil using geosynthetics with special reference to railway engineering.* Ground Improvement, 2007. **11**(1): p. 27-43.

32. Abadi, T., L. Le Pen, A. Zervos, and W. Powrie, *A Review and Evaluation of Ballast Settlement Models using Results from the Southampton Railway Testing Facility (SRTF).* Procedia Engineering, 2016. **143**: p. 999-1006.

33. Partington, W., *TM-TS-097: Track deterioration study - Results of the track laboratory experiments*. 1979, British Railway Research: Derby.

34. Frohling, R.D., *Low frequency dynamic vehicle-track interaction: modelling and simulation.* Vehicle System Dynamics, 1998. **29 Suppl.**(1): p. 30-46.

35. Abadi, T., L.L. Pen, A. Zervos, and W. Powrie, *Effect of Sleeper Interventions on Railway Track Performance.* Journal of Geotechnical and Geoenvironmental Engineering, 2019. **145**(4).

36. Shenton, M., *Ballast Deformation and Track Deterioration*, in *Track Technology*. 1984, Thomas Telford Ltd: London.

37. Zhang, X., C. Zhao, W. Zhai, C. Shi, and Y. Feng, *Investigation of track settlement and ballast degradation in the high-speed railway using a full-scale laboratory test.* Proceedings of the Institution of Mechanical Engineers, Part F: Journal of Rail and Rapid Transit, 2019. **233**(8): p. 869-881.

38. Okabe, Z. and N. Yasuyama, *Laboratory Investigation of Railroad Sub-Ballast*. 1961. p. 33-45.

39. Knight, J.B., C.G. Fandrich, C.N. Lau, H.M. Jaeger, and S.R. Nagel, *Density relaxation in a vibrated granular material.* Physical review E, 1995. **51**(5): p. 3957-3963.

40. Saussine, G., J. Quezada, P. Breul, and F. Radjai, *Railway Ballast Settlement: A New Predictive Model*, in *Second International Conference on Railway Technology: Research, Development and Maintenance*. 2014, Civil-Comp Press: Ajaccio.

41. Grossoni, I., S. Iwnicki, Y. Bezin, and C. Gong, *Dynamics of a vehicle–track coupling system at a rail joint.* Proceedings of the Institution of Mechanical Engineers, Part F: Journal of Rail and Rapid Transit, 2015. **229**(4): p. 364-374.

42. Sato, Y., *Optimization of track maintenance work on ballasted track*, in *World Congress on Railway Research (WCRR'97)*. 1997: Florence. p. 405-411.

43. Milne, D.R.M., L.M. Le Pen, D.J. Thompson, and W. Powrie, *Properties of train load frequencies and their applications.* Journal of Sound and Vibration, 2017. **397**: p. 123-140.

44. Powrie, W., L. Le Pen, D. Milne, and D. Thompson, *Train loading effects in railway geotechnical engineering: Ground response, analysis, measurement and interpretation.* Transportation Geotechnics, 2019. **21**: p. 100261.

45. Al Shaer, A., D. Duhamel, K. Sab, G. Forêt, and L. Schmitt, *Experimental settlement and dynamic behavior of a portion of ballasted railway track under high speed trains.* Journal of Sound and Vibration, 2008. **316**(1-5): p. 211-233.

46. Sussman, T., W. Ebersöhn, and E. Selig, *Fundamental nonlinear track load-deflection behavior for condition evaluation.* Transportation Research Record, 2001. **1742**(1): p. 61-67.

47. Abadi, T., L. Le Pen, A. Zervos, and W. Powrie, *Measuring the area and number of ballast particle contacts at sleeper/ballast and ballast/subgrade interfaces.* The International Journal of Railway Technology, 2015. **4**(2): p. 45-72.

48. Bruni, S., A. Collina, and R. Corradi, *Numerical modelling of railway runnability and ballast settlement in railroad bridges.* EURODYN 2002, 2002: p. 1143-1148.

49. Ferreira, P.A. and A. López-Pita, *Numerical modeling of high-speed train/track system to assess track vibrations and settlement prediction.* Journal of Transportation Engineering, 2012. **139**(3): p. 330-337.

50. Le Pen, L., D. Milne, D. Thompson, and W. Powrie, *Evaluating railway track support stiffness from trackside measurements in the absence of wheel load data.* Canadian Geotechnical Journal, 2016. **53**(7): p. 1156-1166.

List of symbols

Symbol	Definition
A	A material parameter with units of stress, interpreted as a plastic modulus
A_s	Area of the sleeper soffit.
C, C_1, C_2	Empirically-determined curve fitting constants in empirical ballast settlement equations
E^e	Elastic stiffness
E^e_{ref}	Reference value of elastic stiffness
F_b	Force at the ballast level and is the a
K_1, K_2, K_3	Constants with units of kPa, m^{-1} and no units respectively in Fröhling's equation
N	Number of load cycles
N_0	Empirically-determined curve fitting constant in empirical ballast settlement equation
P_{dyn}	Dynamic wheel load in Fröhling's equation
P_{ref}	Reference wheel load used in connection with Fröhling's equation
P_{th}	Threshold pressure (stress) in Sato's equation
S_N	Settlement after N load cycles
S_0	Settlement after one loading cycle
S_1	Settlement after the first load cycle
S_2	Empirically-determined curve fitting constant in empirical ballast settlement equation
a, b, c, d, e	Empirically-determined curve fitting constants in empirical ballast settlement equations
$d_{b,max}$	Maximum elastic sleeper deflection in Guerin's equation
h_0^p	Scaling parameter used in Equation (8)
k	An internal parameter loosely quantifying how the properties of the material change during the course of deformation; it is assumed that $k \equiv \varepsilon^p$ as a first approximation.
k_{2mi}	Measured average track stiffness (MN/m) at a particular sleeper (used in Fröhling's equation)
w	Exponent in Fröhling's equation
ΔN	Increment of number of load cycles
ΔS	Increment of plastic settlement
α, β	Empirically-determined curve fitting constant in empirical ballast settlement equations
ε	Total strain
ε^e	Elastic strain
ε^p	Plastic strain
ε_N	Strain after N loading cycles
$\varepsilon_1^p, \varepsilon_2^p$	Pastic strains at the start and end of a load cycle $\sigma_1 \rightarrow \sigma_2 \rightarrow \sigma_1$
σ	Vertical stress
σ_t	Threshold stress

$\sigma_{t,0}$	Initial value of the threshold stress at $E^e = E^e_{ref}$.
$\sigma_{u,ref}$	Value of the ultimate stress at $E^e = E^e_{ref}$
$\sigma_{t,ref}(\varepsilon^p)$	Captures the (assumed hyperbolic) dependence of σ_t on the plastic strain
σ_u	Ultimate (failure) vertical stress
σ_l, σ_2	Upper and lower limits of load in a loading cycle
	A superimposed dot indicates increments of a quantity
	Other symbols are defined with reference to specific equations in Appendix 1

APPENDIX: SUMMARY OF SETTLEMENT EQUATIONS IN THE LITERATURE

Taufan Abadi (University of Southampton), Ilaria Grossoni, William Powrie, Antonis Zervos, Yann Bezin, Louis Le Pen

Reference	Equation	Variable declaration / values of constants	Based on settlement after first cycle (Y/N)	Includes load explicitly ?(Y/N)	Derivation (lab test/on track test/computer modelling)	Type of test (lab)	Additional information available
TYPE 1: LOGARITHMIC FORM							
Okabe (1961)	$y = C_1 - C_2\, e^{-\alpha x} + \beta x$ if there is no variation in train load $y = C_1 - C_1\, e^{-\alpha x} + \beta x$ $y = C_1(1 - e^{-\alpha x}) + \beta x$	α, β, C_1, C_2 = constants	Y	N	Lab	Large scale test	Two limestone ballasts used
ORE (1970)	$\varepsilon_N = 0.082\,(100n - 38.2)(\sigma_1 - \sigma_3)^2 \times$ $(1 + 0.2 \log N)$	n= porosity σ_1, σ_3= principal stresses.	N	Y	Lab	Triaxial test	
Shenton (1978)	$\varepsilon_N = \varepsilon_1(1 + 0.2\, \log_{10} N)$	ε_1 = strain at 1st cycles	Y	N	Lab	Triaxial test	0.4 was suggested by Knutson (1976) as constant
Henn (1978)	$S = c_1 + c_2\, p + c_3\, p^{1.21} \ln N$	p= sleeper/ballast pressure c_1 to c_3 = constants	N	Y			
Holzlohner (1978)	$S = R_s\, \ln\left(\dfrac{N_{total}}{N_i}\right)$	R_s= settlement rate.	N	N			

Alva-Hurtado & Selig (1981)	$\varepsilon_N = (0.85 + 0.38 \ \log \ N)\ \varepsilon_1 + (\varepsilon_1)^2$ $(0.05 - 0.09 \log N)$	ε_1 = strain at 1st cycles	Y	N	Lab	Triaxial test	Based on drained tests on granite ballast (150 mm diameter and 300 mm height).
Shenton (1984)	$S = K_s \ \dfrac{A_e}{20} \left(\begin{array}{c} (0.69 + 0.028L)\ N^{0.2} + \\ (2.7 \times 10^{-6})N \end{array} \right)$	A_e = average axle load L = tamping lift K_s = empirical constant	N	Y	On track		
Hettler (1984)	$S_N = r\ (F)^{1.6}\ (1 + C\ \ln\ (N))$	F = loading force C = 0.25 to 0.55 r = 0.00095 (mm/kN$^{1.6}$)	N	Y	Lab		
Stewart & Selig (1984)	$\varepsilon_N = \varepsilon_1 \big(1 + C\ \log_{10} N\big)$	ε_1 = strain at the first cycle C = 0.29	Y	N	Lab		
	$d_N = d_1 \big(1 + C_b \log N\big)$	C_b = 0.35 (compacted) and 0.63 (uncompacted)	Y	N	Lab	Reduced scale ballast box test	
Jeffs and Marich (1987)	If N<200,000: $S_N = C_1 + C_2 \log N + C_3 N$ If N>200,000: $S_N = C_4 + C_5 N$	C_1 to C_5 = constants.			Lab	Reduced scale ballast box test	Tests run at 6Hz with 32,5 tons axle load
Selig & Waters (1994)	$\varepsilon_N = \varepsilon_1 \big(1 + C\ \log N\big)$	C = 0.25 (compacted) or 0.4 (uncompacted)	Y	N	Lab	Triaxial test	

Indraratna et al (1997)	$S_N = S_1(a \log N + 1)$	Loose ballast (13.8kN/m^3): S_1=2.31 mm and a= 0.345 Dense ballast (15.6kN/m^3): S_1=9.68 mm and a= 0.345.	Y	N	Lab	Large scale ballast box test	Latite ballast under 200km/h and 560kPa load (30 ton axle load)
Fröhling (1998)	$S_N = \left\{ \left[K_1 + K_2 \cdot \left(\frac{k_{2mi}}{K_3} \right) \right] \cdot \frac{P_{dyn}}{P_{ref}} \right\}^w \cdot \ln N$	k_2mi= measured average track stiffness in a particular sleeper bay P_{dyn} = the dynamic wheel load P_{ref} =the reference wheel load (13 tons) K_3 = 1.34; K_1 = 194 K_2=-1.96. w= 0.3.	N	Y	On track		
Neidhart (2001)	$S = S_1 + \frac{c \log N}{1 + d \log N}$	c, d = coefficients	Y	N			
Indraratna & Wadud Salim (2003)	$S = \alpha + \beta \log N$	α, β = coefficients			Lab	Large scale ballast box test	25 tons axle load, 15 Hz and timber sleeper
Thom & Oakley (2006)	$S = \left[\log_{10} (N) - 2.4 \right]^2$		N	N	Lab	Full scale ballast box test	250 kN axle load.

Thom & Oakley (2006)	$S = \left[\log_{10}(N) - 2.4\right]^2 \left(\dfrac{\sigma}{160}\right)\left(\dfrac{47}{k_s}\right)$	σ= vertical pressure k_s=subgrade stiffness	N	Y	Lab	Full scale ballast box test	
Shahin (2009)	$\varepsilon_B = a\left(\dfrac{\sigma_d}{\sigma_s}\right)^m (1+\ln N)^b$	σ_d= deviatoric stress applied σ_s= compressive strength of ballast For basalt ballast: a=3.38, m=1.13, b=0.523 For granite ballast: a=2.10, m=1.67, b=0.491 For dolomite ballast: a=4.72, m=1.12, b=0.312	N	Y	Lab	Large triaxial test	
Indraratna et al (2013)	$S = a + b\log_{10} N$	a, b = coefficients	N	N	Lab	Large scale ballast box test	20 ton axle load, 100 km/h and timber sleeper used
Indraratna & Nimbalkar (2013)	$S_N = S_1\left(1 + a\ln N + 0.5b\ln N^2\right)$	S_1 = settlement at the first cycle a, b = coefficients	Y	N	Computer modelling		
TYPE 2: EXPONENTIAL FORM							
Selig & Waters (1994)	$S_N = 4.318\,N^{0.17}$				Lab	Large scale ballast box test	Timber sleeper on dolomite ballast with 347kN axle load.

Selig & Waters (1994)	For ballast only: $$\varepsilon_N = 0.0035\ N^{0.21}$$ For sub-ballast only: $$\varepsilon_N = 0.0036\ N^{0.16}$$ For subgrade only: $$S_N = 0.03556\ N^{0.37}$$				On track		Timber sleepers
Sato (1997)	Ballast settlement rate either: $S_i = a\ (p - b)^2$ for $p > b$, or $S_j = A\ p^n$ $$S_N = S_j\ N$$	a, A = coefficients n = power index p = sleeper pressure b = pressure threshold			On track		
Indraratna et al (2007)	$$S_N = S_1 N^y$$	y = coefficient S_1 = settlement at the first cycle	Y	N	Lab	Large scale ballast box test	
Cuellar et al (2011)	$$S_N = 0.07\ N^{0.1625}$$		N	N	Lab	Full scale ballast box test	Bituminous sub-ballast used in various thicknesses
OTHER FORMS							
Guérin, N (1996)	$$dS_N/dN = i \cdot d_{b,max}^{\ j}$$	$i = 0.00000144$ $j = 2.51$	N	Y	Lab	Triaxial test	200 km/h under 17 t axle load
Varandas et al. (2013)	$$S_N = \frac{\gamma}{M_\theta}\ \frac{F_n^{\ \alpha+1}}{(\alpha+1)}\ \sum_{n=1}^{N}\left(\frac{1}{n}\right)^\beta$$	α, β, γ = positive parameters F_n = load M_θ = normalizing parameter			Computer modelling		

| Nimbalkar & Indraratna 2016 | $S_N = S_1(1-e^{-\alpha N})+\beta \ln N$ | Soft alluvial deposit: $\alpha= 0.5$ $\beta=2.04$ Hard rock: $\alpha= 0.5$ $\beta= 1.7$ concrete bridge deck: $\alpha= 0.5$ $\beta= 0.63$ | Y | N | On track | | |